

A Research on the Influence of Flux Air Gaps on Electromagnetic Components of Shunt Reactors

Dang Chi Dung

School of Electrical and Electronic Engineering, Hanoi University of Science and Technology, Vietnam
dung.dangchi@hust.edu.vn

Doan Thanh Bao

Faculty of Engineering and Technology, University of Quy Nhon, Vietnam
doanthanhbao@qnu.edu.vn

Phan Hoai Nam

Faculty of Electrical Engineering, University of Economic and Technical Industries, Vietnam
phnam@uneti.edu.vn

Pham Minh Tu

School of Electrical and Electronic Engineering, Hanoi University of Science and Technology, Vietnam
tu.phamminh@hust.edu.vn

Vuong Dang Quoc

School of Electrical and Electronic Engineering, Hanoi University of Science and Technology, Vietnam
vuong.dangquoc@hust.edu.vn (corresponding author)

Received: 31 December 2023 | Revised: 21 January 2024, 30 January 2024, and 31 January 2024 | Accepted: 3 February 2024

Licensed under a CC-BY 4.0 license | Copyright (c) by the authors | DOI: <https://doi.org/10.48084/etasr.6842>

ABSTRACT

This paper introduces an evaluation of the flux air gaps of Shunt Reactors (SRs) to effectively mitigate fringing and leakage fluxes along the height of the iron core. The assessment of these discretely distributed flux air gaps in SRs is a rigorous and challenging process. To define their exact number, the case of one flux air gap is analyzed and investigated to observe/simulate the influence of the flux density distribution and the leakage flux along the air gaps on the reactive power and the operation conditions of the SR. Based on that, to reduce leakage flux, a large flux air gap is divided into smaller ones. Initially, an analytic model is presented to define the main parameters of the SRs. Then, a finite element method is developed to simulate electromagnetic quantities, such as the magnetic flux density, leakage flux, and electromagnetic force. The obtained results can help manufacturers define the exact number of flux air gaps along the iron core of the SR. From that, a suitable technology can be given in manufacturing high voltage SRs applied to high or super high voltage transmission lines.

Keywords-shunt reactors; leakage flux; electromagnetic force; flux air gaps, analytical method; finite element method

I. INTRODUCTION

Shunt Reactors' (SRs) purpose is to absorb voltage fluctuations resulting from variations in load and capacitive load on high-voltage transmission lines. The SRs can be continuously switched on based on the load condition of the power transmission lines. They play a crucial role in mitigating transients entering the circuit, with inrush current being a key

consideration. So far, many applications of SRs in high-voltage power systems have been studied. Authors in [1, 3] applied the Finite Element Method (FEM) to study the properties and phenomena of the SRs used in high voltage systems. In [4-9], the FEM was developed to formulate the Maxwell stress tensor for calculating the electromagnetic parameters of the SR. The relation of leakage and fringing inductances were also established. In [10], the required parameters are defined via the

analytical approach based on the theory of magnetic circuit models. In [11], the arrangement of flux air gaps along the iron core was orchestrated to alleviate the impact of fringing and leakage fluxes around these gaps. However, this research has not shown the exact number of flux air gaps that need to be split from a large flux air gap into smaller ones, something that still constitutes a big challenge for researchers and designers.

In this paper, the analytical computation process is first considered to define the main parameters of the SR. Then, a finite element model is developed to investigate and evaluate the leakage and fringing flux distribution along the flux air gaps and the electromagnetic forces acting directly on the core blocks of the SR. Thus, the exact number of flux air gaps of the SR can be obtained helping researchers and manufactures to choose a suitable technology in designing and manufacturing SRs. The proposed method is applied and validated on the practical problem of 17 MVar, 500kV.

II. BACKGROUND ON SHUNT REACTORS

A. Determination of the Main Dimensions of the SR

In this part, a single phase SR (reactive power of 17 MVar, voltage of $500/\sqrt{3}$, frequency of 50 Hz) with a single and multi-flux air gap is considered. The model of this SR is given in Figure 1.

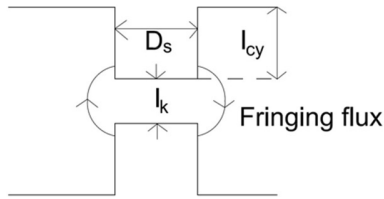


Fig. 1. Model of the flux air gap of the SR.

The electromagnetic force (EMF) and the electric current are provided in [12-14]. The volume of the air gap (V_k) is determined as [6, 12-14]:

$$V_k = A_k \cdot l_k = \frac{Q}{\mu_0 \cdot f \cdot B_m^2} \quad (1)$$

The dimension of core block (D_c) can be defined via the term A_k :

$$D_c = \sqrt{\frac{4 \cdot A_k}{\pi}} \quad (2)$$

The winding inductance is calculated by [3-5]:

$$L = N^2 \cdot \mu_0 \cdot \left(\frac{A_k}{l_k}\right) = \left(\sqrt{\frac{L}{\mu_0 \cdot \left(\frac{A_k}{l_k}\right)}}\right)^2 \cdot \Phi_{leak} \quad (3)$$

where Φ_{leak} is the leakage flux and l_k is the thickness of the air gap.

B. Analysis of the Flux Air Gap of the Shunt Reactor

In this part, the impact of the number of flux air gaps on the iron core SR is analytically considered. Figure 2 shows an SR

with a single flux air gap. From Figure 2, the flux density (B) at the flux air gap is computed by [10, 15]:

$$B = \frac{\mu_0 \cdot F}{(l_k + \pi \cdot r)} \quad (4)$$

where F is the magnetomotive force (MMF) and r is the radius of the leakage flux (Φ_{leak*}).

For a single flux air gap, the Φ_{leak*} can be defined as [6, 10]:

$$\Phi_{leak*=1} = \frac{\int B dS}{F} = \mu_0 \cdot D_s \cdot \ln\left(1 + \frac{\pi \cdot l_s}{2 \cdot l_k}\right) \quad (5)$$

where l_s is the thickness of core block.

For the multi-flux air gap, the $\Phi_{leak*>1}$ is defined as [10]:

$$\begin{aligned} \Phi_{leak*>1} &= \frac{\int B dS}{F} = \int_0^{l_{cy}} \frac{\mu_0 \pi D_s}{((g-1)l_s + g l_k + \pi \cdot r)} d_r \\ &= \frac{\mu_0 \cdot D_c}{\pi} \cdot \ln\left(1 + \frac{\pi \cdot l_s}{(g-1)l_s + g l_k}\right) \end{aligned} \quad (6)$$

where g is the air gap number.

The total magnetic flux (Φ_{total}) takes the fringing flux into account and is expressed as:

$$\Phi_{total} = \frac{\Phi_{g+} + \Phi_{leak*=1}}{g} + \Phi_{leak*>1} \quad (7)$$

Based on the analytic theory developed above, the results of the main parameters of the proposed SR of 17 MVar are displayed in Table I.

TABLE I. ANALYTICAL RESULTS

Parameter	Symbol	Value
Reactive power	Q (MVar)	17
Rated voltage	U (kV)	$500/\sqrt{3}$
Rated current	I (A)	58.89
Total inductance	L_{total} (H)	15.6
Fringing inductance	$L_{fringing}$ (H)	4.9
Gap inductance	L_{gap} (H)	9.6
Core dimension	D_s (mm)	572
Height of core	H_s (mm)	1579
Total air gap	l_k (mm)	264
Turn number	N (turn)	2761
Width of winding	Wd (mm)	218
Height of winding	Hd (mm)	1309
Gaps	g	6

III. FINITE ELEMENT METHOD

A. Maxwell's Equations

The Maxwell's equations and behavior laws are written in Euclidean space \mathbb{R}^3 as [10, 12]:

$$\text{curl } \mathbf{H} = \mathbf{J}_s \quad (11a)$$

$$\text{curl } \mathbf{E} = -j\omega \mathbf{B} \quad (11b)$$

$$\text{div } \mathbf{B} = 0 \quad (11c)$$

$$\mathbf{B} = \mu \mathbf{H} \quad (12a)$$

$$\mathbf{J} = \sigma \mathbf{E} \quad (12b)$$

where \mathbf{H} is the magnetic field (A/m), \mathbf{B} is the magnetic flux density (T), \mathbf{E} is the electric field (V/m), \mathbf{J}_s is the current density (A/m²), \mathbf{J} is the eddy current density (A/m²), and μ and σ are respectively the relative permeability and the electric conductivity (S/m).

Equations (11a) and 11(b) are solved with boundary conditions (BCs) defined on Γ , they are expressed as [11, 12]:

$$\mathbf{n} \times \mathbf{H}|_{\Gamma_h} = 0 \tag{13a}$$

$$\mathbf{n} \cdot \mathbf{B}|_{\Gamma_e} = 0 \tag{13b}$$

where \mathbf{n} is the unit normal exterior to Ω (with $\Omega = \Omega_c \cup \Omega_c^c$). Domain Ω_c is the conducting region and Ω_c^c is the non-conducting regions.

The fields \mathbf{H} , \mathbf{B} , \mathbf{E} , and \mathbf{J} belong to the function spaces $\mathbf{F}_h(\text{curl}; \Omega)$ and $\mathbf{F}_e(\text{div}; \Omega)$ that are satisfied. Tonti's diagram [6] is illustrated in Figure 2, with $\mathbf{H} \in \mathbf{F}_h(\text{curl}; \Omega)$, $\mathbf{E} \in \mathbf{F}_e(\text{curl}; \Omega)$, $\mathbf{J} \in \mathbf{H}(\text{div}; \Omega)$ and $\mathbf{B} \in \mathbf{F}_e(\text{div}; \Omega)$.

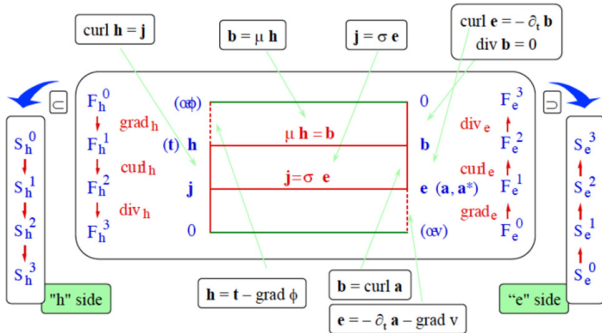


Fig. 2. Tonti's diagram.

B. Weak Formulations of Magnetic Vector Potential

The field \mathbf{B} in (11c) is derived from a vector potential \mathbf{A} :

$$\mathbf{B} = \text{curl } \mathbf{A} \tag{14}$$

From (11b) and (14), the field \mathbf{E} can be defined via the electric scalar potential v :

$$\mathbf{E} = -\partial_t \mathbf{A} - \text{grad } v \tag{15}$$

Based on the Ampere's law (11a), the weak formulation of magnetic vector potential is written as [10, 12]:

$$\frac{1}{\mu} \oint_{\Omega} (\text{curl } \mathbf{A} \cdot \text{curl } \mathbf{t}') d\Omega - \sigma \oint_{\Omega_c} (\partial_t \mathbf{A} \cdot \text{curl } \mathbf{t}') d\Omega_c + \sigma \oint_{\Omega_c} (\text{grad } v \cdot \text{curl } \mathbf{t}') d\Omega_c + \int_{\Gamma} (\mathbf{n} \times \mathbf{H}) \cdot \mathbf{t}' d\Gamma = \oint_{\Omega_s} (\mathbf{J}_s \cdot \mathbf{t}') d\Omega_s, \forall \mathbf{t}' \in \mathbf{F}_e^0(\text{curl}, \Omega) \tag{16}$$

where the function space $\mathbf{F}_e^0(\text{curl}, \Omega)$ defined in Ω contains the basis functions for \mathbf{A} and for the test function \mathbf{t}' .

The inductance value \mathbf{L} is defined via the post processing:

$$\mathbf{L} = \frac{\oint_{\Omega} \mathbf{H} \cdot \mathbf{B} d\Omega}{I^2} \tag{17}$$

IV. NUMERICAL TEST

The tested problem is a single-phase high voltage SR with a power of 17 MVar, voltage of 500/ $\sqrt{3}$ V and frequency of 50 Hz. The main parameters of the SR are already designed in Table I. The model of the single phase SR is depicted in Figure 3. The distribution of magnetic vector potential and magnetic flux density in the iron cored of the SR with a single flux air gap is presented in Figure 4.

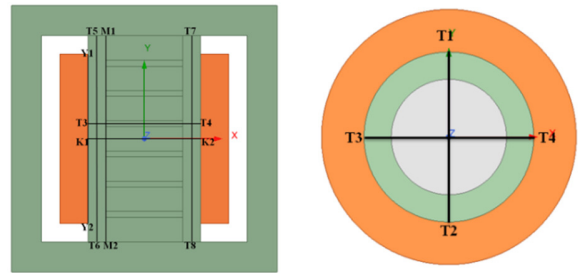


Fig. 3. Modeling of a single phase 16 MVar SR.

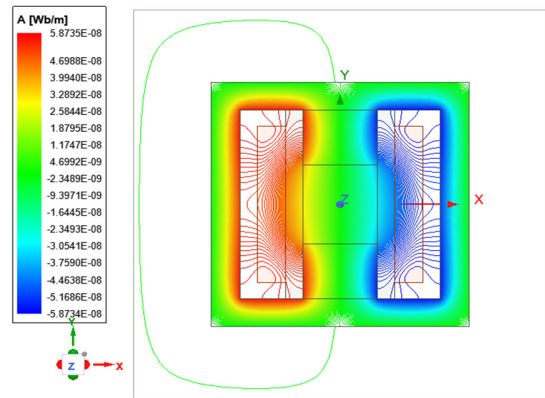


Fig. 4. Distribution of magnetic vector potential.

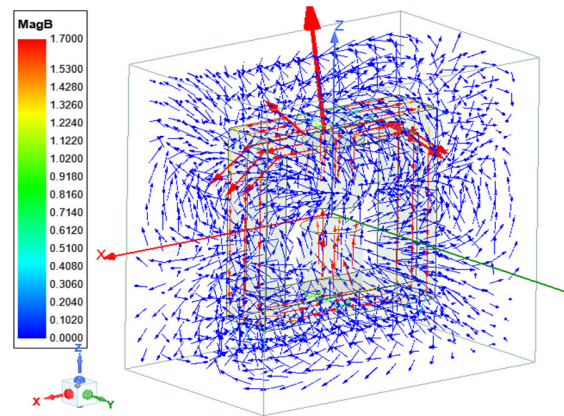


Fig. 5. Distribution of different inductance components.

It can be seen that the fringing flux appears in the air gaps along the core blocks and the height of the winding is very large, increasing the fringing/leakage inductance in the flux air

gaps as portrayed in Figure 5. The maximum value on magnetic flux density $\mathbf{B} = \text{curl} \mathbf{A}$ is 1.7 T. The obtained results indicate that when the circuit material has a high permeability and the air gap is sufficiently small, the magnetic flux is predominantly distributed within the core of the circuit without significant leakage. However, for a single flux air gap, the magnetic flux leakage will be very large, leading to a large leakage inductance. This influences directly the operational performance of the SR. In order to reduce the distribution of magnetic flux density ($\mathbf{B} = \text{curl} \mathbf{A}$) and leakage/fringing flux along the core block and the height of the winding, a divided technique of the flux air gap is performed. In this study, a single flux air gap is split into six portions. Each portion has magnetic flux density and electromagnetic force acting directly on each core block.

The distribution of flux density along the core blocks at lines T1T2 and T3T4 with the different flux air gaps is depicted in Figure 6. It can be seen that for one and two air gaps, the flux density reaches 0.8 T in the central region of the core blocks and strongly decreases towards both edges of the core blocks. When the flux air gap is bigger than two gaps, the flux density value is reduced to 0.75 T. Of course, the minimum value at the corner of the core block for the six flux air gaps is also reduced to 0.05 T.

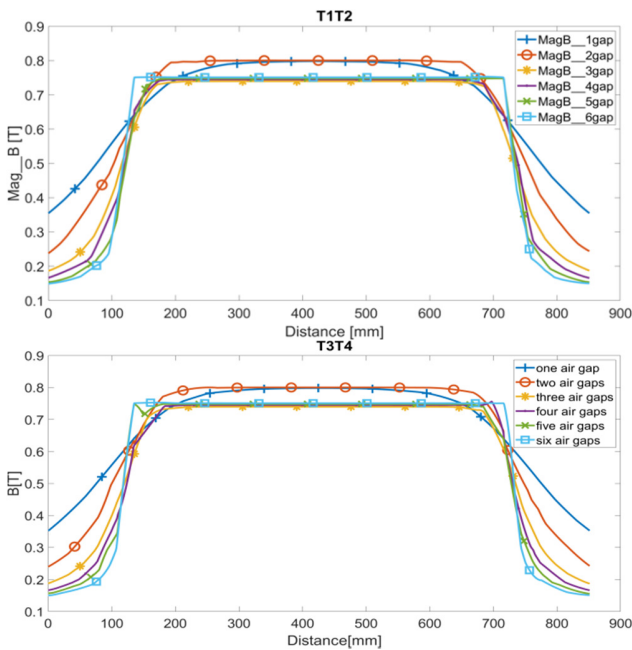


Fig. 6. Flux density in lines T1T2 (top) and T3T4 (bottom) along the core block of the SR.

The distribution of flux density along the core blocks in line T5T6 with different flux air gaps is exhibited in Figure 7. The maximum flux density is 0.55 T for a single flux air gap, and 0.18 T for six flux air gaps, decreased by 70% compared to the case of a single-flux air gap. Figure 8 shows the flux density in the line Y1Y2 along the winding of the SR. It can be observed that the maximum flux density is 0.35 T for a single flux air gap, and 0.14 T for six flux air gaps, decreased by 60%.

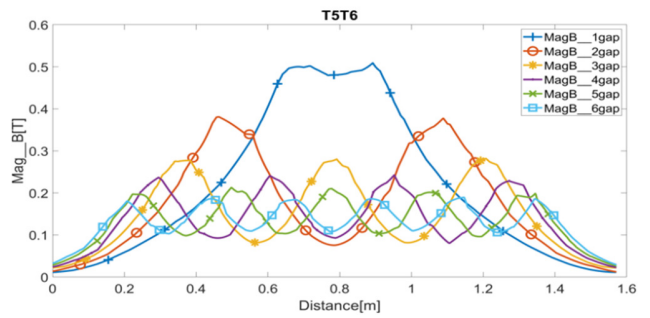


Fig. 7. Flux density in the line of T5T6 along the core block of SR with different flux air gaps.

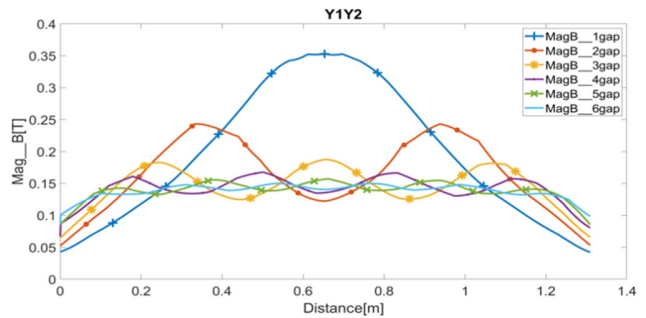


Fig. 8. Flux density in lines Y1Y2 along the core block of the SR with different flux air gaps.

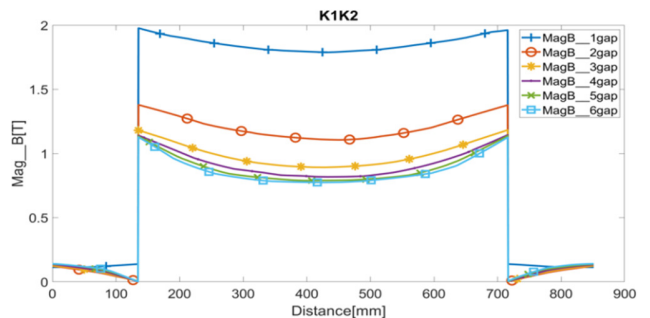


Fig. 9. Flux density in lines K1K2 across the core block of the SR with different flux air gaps.

The flux density in the lines K1K2 across the core block of the SR with different flux air gaps along the winding of the SR is presented in Figure 9. The results indicate that for six flux air gaps, the flux density is equal to 1.1 T at the corner of the core block and 0.8 T at the core middle, while for a single flux air gap, its value is 1.8 T at the corner and 1.75 T at the core middle. This means that it is reduced by 0.6 times compared to the single flux air gap case. In a similar analysis, the distribution of the flux density along the core blocks at the line M1M2 with six air gaps is pointed out in Figure 10. The EMF on the segment K1K2 in the case of six flux air gaps is depicted in Figure 11. It can be seen that for one flux air gap, the force near the corner of the core block is very large and reaches approximately 3.1×10^5 N at the corner. It should be noted that when the number of air gaps increases, the force decreases. Specifically, when the number of air gaps is 5, the value of the force change is very small in comparison with the case of a single flux air gap.

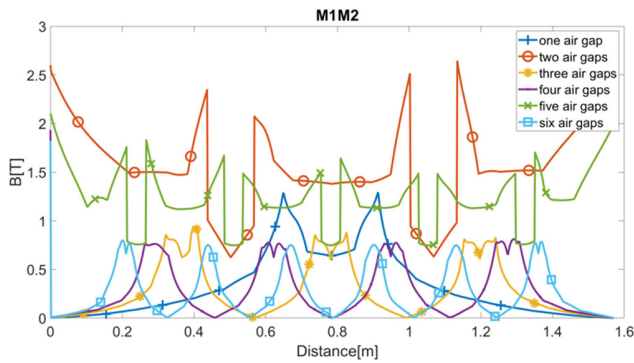


Fig. 10. Fluxensity in lines M1M2 along the core block of the SR with different flux air gaps.

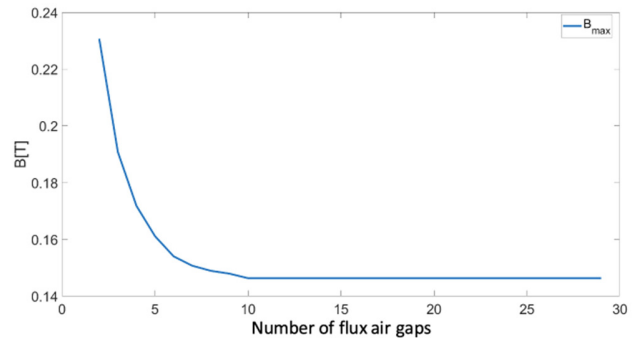


Fig. 12. Relationship between flux density and the number of flux air gaps.

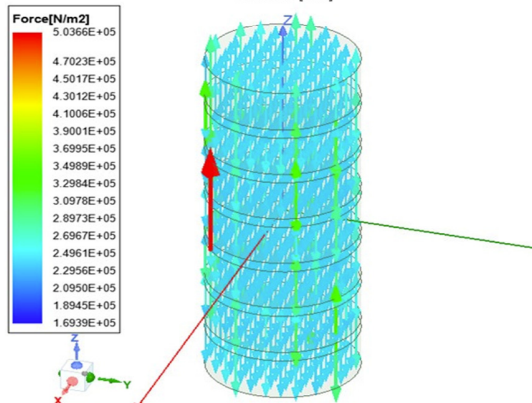
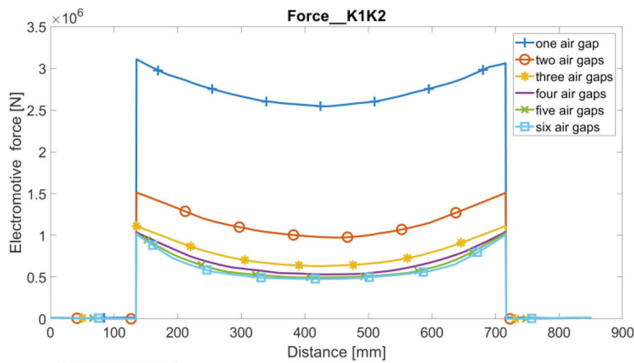


Fig. 11. Electromagnetic force at the line K1K2 acting on the core block with six flux air gaps.

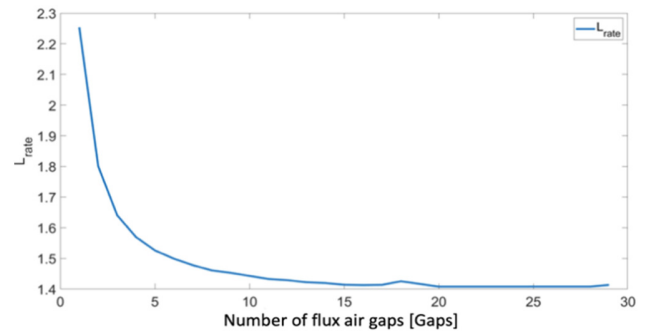


Fig. 13. Relationship between the rated inductance and the flux air gap number.

Based on these values, the suitable number of flux air gaps is proposed for researchers and manufactures who want to define the reactive power and current during the operation of the SRs.

V. CONCLUSION

The current article has successfully combined the analytical method and finite element modeling to determine the impact of the number of air gaps on flux density, electromagnetic force, and inductance values of the SR. To achieve this, the analytical method was first developed based on the results of previous studies to determine the required parameters of the SR as shown in Table I. Subsequently, a finite element model was proposed to simulate the electromagnetic parameters. The acquired results of the paper allow to:

- Determine the exact number of air gaps based on the total inductance ratio to air gap inductance.
- Analyze the distribution of the flux density from the winding in the air gap, both radially and along the coil winding and the core blocks.
- Investigate the distribution of EMFs acting on the surface of the core blocks corresponding to different numbers of air gaps.
- Establish the values of air gap inductance and explore the relationships between the inductance values and the number of air gaps.

TABLE II. FLUX DENSITY AND INDUCTANCE WITH DIFFERENT FLUX AIR GAPS

Air gap no	B (T)	L _{total} (H)	L _{gap} (H)	L _{rated} = L _{total} /L _{gap}
2	0.230	18.44	10.24	1.80
4	0.171	16.06	10.23	1.59
6	0.154	15.32	10.22	1.50
8	0.149	14.93	10.22	1.46
10	0.146	14.77	10.22	1.44
12	0.146	14.60	10.22	1.43
16	0.146	14.86	10.47	1.43
20	0.146	14.44	10.22	1.41
25	0.146	14.38	10.21	1.41
29	0.146	14.35	10.20	1.41

The obtained results may serve as reference data, assisting researchers and manufacturers in selecting suitable flux air gaps and insulation materials for SRs in practice.

ACKNOWLEDGMENT

This research is funded by the Hanoi University of Science and Technology (HUST) under project number T2023-PC-042.

REFERENCES

- [1] W. Chen, H. Chen, T. Lu, and W. Zhou, "Ultra-high voltage controllable shunt reactor," *High Voltage Engineering*, vol. 31, no. 11, pp. 26–27, Nov. 2005.
- [2] W. Xu, S.-M. Chen, and H. Jinliang, "Research on switching overvoltage caused by faults in 1000kV UHV AC transmission line," *Power System Technology-Beijing*, vol. 29, no. 21, Nov. 2005.
- [3] A. Donuk, "Modeling and design of iron-core shunt reactors with discretely distributed air-gaps," Ph.D. dissertation, Middle East Technical University, 2012.
- [4] D. I. Zaikin, S. Jonassen, and S. L. Mikkelsen, "An Air-Gap Shape Optimization for Fringing Field Eddy Current Loss Reductions in Power Magnetics," *IEEE Transactions on Power Electronics*, vol. 34, no. 5, pp. 4079–4086, Feb. 2019, <https://doi.org/10.1109/TPEL.2018.2868289>.
- [5] Q. Y. Zhou, Q. Guo, G. Q. Bu, and L. G. Ban, "Application of controllable reactors in China's power grid at extra and ultra voltage level," *Proceedings of the Chinese Society of Electrical Engineering*, vol. 27, no. 7, pp. 1–6, Mar. 2007.
- [6] H. De Gerssem and K. Hameyer, "A finite element model for foil winding simulation," *IEEE Transactions on Magnetics*, vol. 37, no. 5, pp. 3427–3432, Sep. 2001, <https://doi.org/10.1109/20.952629>.
- [7] H. B. Duc, T. P. Minh, T. P. Anh, and V. D. Quoc, "A Novel Approach for the Modeling of Electromagnetic Forces in Air-Gap Shunt Reactors," *Engineering, Technology & Applied Science Research*, vol. 12, no. 1, pp. 8223–8227, Feb. 2022, <https://doi.org/10.48084/etasr.4692>.
- [8] T. P. Minh, H. B. Duc, and V. D. Quoc, "Analysis of Leakage Inductances in Shunt Reactors: Application to High Voltage Transmission Lines," *Engineering, Technology & Applied Science Research*, vol. 12, no. 3, pp. 8488–8491, Jun. 2022, <https://doi.org/10.48084/etasr.4826>.
- [9] P. M. Tú, V. D. Quoc, and B. Đ. Hùng, "Study of number and size of air-gaps in core of shunt reactors in transmission lines of high and super high voltages," *Journal of Military Science and Technology*, no. 80, pp. 23–30, Jun. 2022, <https://doi.org/10.54939/1859-1043.j.mst.80.2022.23-30>.
- [10] T. P. Minh, "Computation and Simulation of Shunt Reactors by an Analytic Method and Finite Element Method-Application to Transmission Lines of High and Super High Voltages," *Journal of Military Science and Technology*, no. 74, pp. 36–43, Aug. 2021.
- [11] T. P. Minh *et al.*, "Finite Element Modeling of Shunt Reactors Used in High Voltage Power Systems," *Engineering, Technology & Applied Science Research*, vol. 11, no. 4, pp. 7411–7416, Aug. 2021, <https://doi.org/10.48084/etasr.4271>.
- [12] K. Dawood, G. Komurgoz, and F. Isik, "Modeling of Distribution Transformer for Analysis of Core Losses of Different Core Materials Using FEM," in *2019 8th International Conference on Modeling Simulation and Applied Optimization (ICMSAO)*, Manama, Bahrain, Apr. 2019, pp. 1–5, <https://doi.org/10.1109/ICMSAO.2019.8880392>.
- [13] F. Yuan *et al.*, "Thermal Optimization for Dry Type Air Core Reactor Base on FEM," in *2018 21st International Conference on Electrical Machines and Systems (ICEMS)*, Jeju, Korea (South), Jul. 2018, pp. 1726–1730, <https://doi.org/10.23919/ICEMS.2018.8549257>.
- [14] S. Magdaleno-Adame, R. Escarela-Perez, J. C. Olivares-Galvan, E. Campero-Littlewood, and R. Ocon-Valdez, "Temperature Reduction in the Clamping Bolt Zone of Shunt Reactors: Design Enhancements," *IEEE Transactions on Power Delivery*, vol. 29, no. 6, pp. 2648–2655, Sep. 2014, <https://doi.org/10.1109/TPWRD.2014.2322994>.
- [15] A. Najafi and I. Iskender, "Comparison of core loss and magnetic flux distribution in amorphous and silicon steel core transformers," *Electrical Engineering*, vol. 100, no. 2, pp. 1125–1131, Jun. 2018, <https://doi.org/10.1007/s00202-017-0574-7>.